IOP Publishing J. Phys. D: Appl. Phys. 59 (2026) 115107 https://doi.org/10.1088/1361-6463/ae4ef9

Journal of Physics D: Applied Physics



OPEN ACCESS

RECEIVED
6 May 2025

REVISED
18 February 2026

ACCEPTED FOR PUBLICATION
9 March 2026

PUBLISHED
20 March 2026



PAPER

# Wide tunability of zincblende InGaN/GaN quantum wells grown by metal–organic vapour phase epitaxy

D Dyer[1], W R Fieldhouse-Allen[1], S A Church[1], M J Kappers[2], M Frentrup[2], P Vacek[2], D J Wallis[2,3], R A Oliver[2] and D J Binks[1,*]

[1] Department of Physics and Astronomy & Photon Science Institute, University of Manchester, Manchester M13 9PL, United Kingdom
[2] Department of Materials Science and Metallurgy, University of Cambridge, Cambridge CB3 0FS, United Kingdom
[3] Centre for High frequency Engineering, Cardiff University, Cardiff CF24 3AA, United Kingdom
[*] Author to whom any correspondence should be addressed.

**E-mail:** david.binks@manchester.ac.uk

**Keywords:** zincblende, InGaN/GaN, quantum wells, growth temperature

Supplementary material for this article is available online

## Abstract

It is shown that for zincblende InGaN/GaN quantum wells (QWs) produced by metal–organic vapour phase epitaxy, reducing the growth temperature from 740 °C to 684 °C tunes the emission from the blue to the orange region of the visible spectrum. The emission spectrum was found to be independent of the excitation density at each growth temperature, consistent with the QWs being free of significant internal polarisation fields. The spectrally integrated emission intensity at 300 K grows from 22% to 34% of its value at 11 K as the peak emission energy decreases from 2.75 eV to 2.0 eV; this reduction in thermal quenching as the emission energy decreases is attributed to a significant lessening of thermionic emission.

## 1. Introduction

Current commercially-produced nitride-based LEDs utilise *c*-plane wurtzite (wz) phase InGaN/GaN quantum wells (QWs) as the active region and exhibit high efficiency in the blue spectral range. However, the efficiency of these devices reduces significantly as the emission is tuned to longer wavelengths [1]. The increased indium content needed to reach longer wavelengths strengthens the quantum-confined Stark effect (QCSE) present in the material [2], which limits the rate of radiative recombination. To achieve a higher indium content in the QW layers, a lower temperature must be used for the QW growth, since In forms weaker metal-N bonds compared to Ga and hence desorbs more rapidly from the surface at high temperatures [3]. As a side effect, the lower growth temperature may lead to a higher density of unwanted non-radiative point defects in the material, hampering the device performance further [4].

An attractive alternative for longer wavelength emitters is the zincblende (zb) phase of GaN, which lacks the QCSE present in the wz phase when grown along the [001] direction [5–7]. Zb-GaN also has an intrinsically lower bandgap than its wz counterpart [8] (3.3 eV and 3.5 eV at low temperature) so that reduced indium content is needed in the QWs. Such QWs, when grown by molecular beam epitaxy (MBE) [9–11], have demonstrated PL emission that covers the visible spectrum at temperatures $\leqslant$10 K. However, for zb-LEDs to compete commercially with wz-LEDs, it is crucial that the fabrication of zb-LED devices are compatible with the current industry standard growth technique, metal–organic vapour phase epitaxy (MOVPE), to enable large-scale manufacturing of zb devices. Previously, the efficiency of blue-emitting MOVPE-grown zb-QWs has been studied, including its dependence on well width and number [12] and on excitation density [13]. In this article, tuning of the emission of MOVPE-grown zb-InGaN/GaN QWs from blue to orange is demonstrated and its temperature- and excitation-density dependence investigated using temperature-, excitation- and time-dependent photoluminescence (PL) studies and PL mapping.

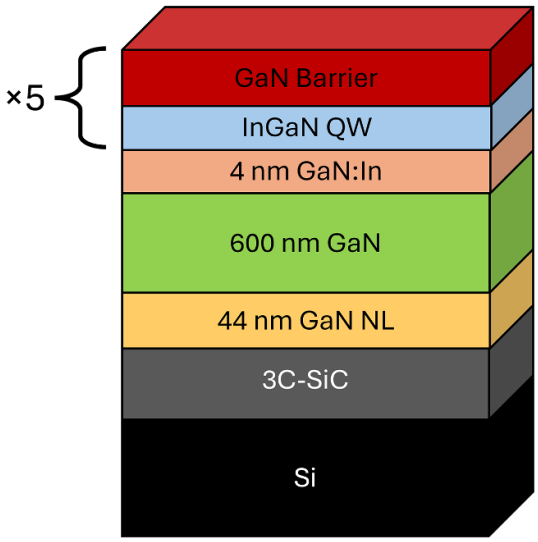


**Figure 1.** Diagram of QW samples studied in this investigation.

## 2. Experimental methods

The samples investigated in this manuscript, shown schematically in figure 1, were grown by MOVPE on 3 C-SiC/Si (001) substrates with a 4° miscut towards [1-10] using an Aixtron 1 × 6in. close-coupled shower head reactor. A 44 nm thick GaN nucleation layer was grown on the SiC/Si substrate, followed by a 600 nm thick GaN buffer layer. The thickness of the SiC layer was found to be 3.21 $\mu$m by measuring the fringe spacing in its white light reflectivity spectrum. On top of this was deposited a 4 nm thick GaN:In underlayer prior to the growth of five QWs; the average thicknesses of the barriers and QW layers grown were determined from energy dispersive x-ray (EDX) mapping, as will be discussed in section 3.1. The series consisted of four samples with the QW growth temperature adjusted from 740 °C to 684 °C to vary the indium composition within the layer, and thus tune the emission across the visible spectrum. In contrast, the GaN barriers and GaN: In underlayer were grown at 855 °C for all samples. The structure of these samples was characterised by x-ray diffraction (XRD) using a PIXcel solid-state area detector in a PANalytical Empyrean diffractometer. A Thermo Fisher Scientific Spectra 300 scanning transmission electron microscope (STEM) with a four-segment SuperX detector was also used for structural characterisation by high-angle annular dark-field (HAADF) imaging and EDX mapping.

PL measurements were carried out on the samples using a 26 mW continuous wave HeCd laser, emitting photons with an energy of 3.8 eV to excite the samples above the bandgap of zb-GaN (3.3 eV at low temperature [8]). The HeCd laser was focused to an 80 $\mu$m diameter spot at the sample. The sample emission was focused into and dispersed by a Horiba iHR550 spectrometer and detected with a Horiba Syncerity CCD array. Variable temperature PL measurements were conducted by mounting the samples onto the cold finger of a closed cycle He cryostat, equipped with a thermofoil heater, to vary the sample temperature from 11 K to 300 K. Discrete neutral density filters were employed to vary the excitation power density incident on the samples. Note that for excitation density-dependent PL measurements, a shorter focal length lens was used to achieve a 40 $\mu$m spot size and thus a higher power density at the samples.

Spatially resolved PL measurements were performed to identify intensity variations of the QW emission across the samples. An ultrafast laser (PHAROS by light conversion), frequency-tripled to 343 nm with a repetition rate of 200 kHz, was passed through a confocal microscope, equipped with a 20× objective lens to excite the zb-QW samples. Note the PHAROS laser was defocused to achieve a spot size of 80 $\mu$m at the sample—identical to the spot size used in the temperature-dependent PL measurements. This gave an average excitation power density at the sample of 6.2 W · cm$^{-2}$. The sample emission, collected from a 66 $\mu$m diameter region of the sample, was coupled into a 550 $\mu$m diameter optical fibre with numerical aperture of 0.22, and directed into an Ocean Optics spectrometer to record the emission spectrum. An automated *xyz* translation stage, moved in steps of 70 $\mu$m in *x* and *y*—a distance comparable to the spot size of the laser in the spatially-integrated PL measurements—enabled the QW emission to be mapped across the surface of the samples.

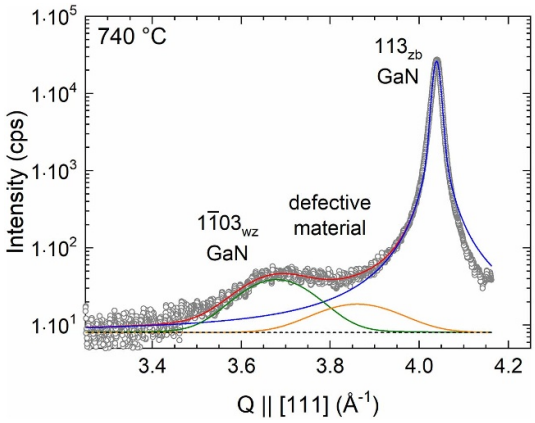


**Figure 2.** X-ray intensity profile along the [111] direction between 113 zb-GaN and 1–103 wz-GaN reflection of the sample grown at 740 °C.

## 3. Results

### 3.1. Structural characterisation

XRD phase analysis was performed for all samples by analysing intensity profiles extracted from reciprocal space maps around the 113 zb-GaN reflection and the nearby 1–103 wz-GaN reflection. Figure 2 shows the XRD spectrum for the sample with the QWs grown at 740 °C, as an example. The spectrum is dominated by the 113 zb peak, which is more than two orders of magnitude greater than the 1–103 wz peak and an intermediate feature attributed to defective material. The phase purity of the sample was determined by fitting peaks to the spectrum as shown and comparing the area under them; in this way, the samples were each found to be >98% zb phase. XRD ω2θ-scans of the on-axis 002 reflection, shown in figure S1 of the supplementary material (SM), are dominated by a broad GaN peak, and a weak InGaN peak on its low diffraction angle shoulder. This shoulder peak shifts to lower diffraction angles as the growth temperature of the InGaN QWs reduces from 740 °C to 684 °C, indicating an increase of the In content in the QWs. However, due to the strong overlap of the GaN and InGaN peaks a quantitative assessment of the indium content from the XRD measurements was not possible. Therefore, additional structural analyses by STEM have been performed.

Figure 3(a) shows a HAADF STEM image of the QWs grown at the highest temperature of 740 °C in which the five InGaN QWs can be seen as bright stripes, indicative of the presence of heavier atoms. EDX was used to map the distribution of indium in the same region as shown in figure 3(b). (Note that the signal in the topmost 20 nm of the image is due to Bremsstrahlung from the Pt coat applied to the sample for these measurements). A line scan was taken over the region and in the direction shown in figure 3(b) to determine the indium concentration in the QWs and their width, and is shown in figure 3(c). The indium content ($x$) in the $In_xGa_{1-x}N$ QWs had a maximum of 5% above the background level and was approximately 1% in the underlayer. The average QW and quantum barrier (QB) widths, as determined from the full width half maximum (FWHM) of the indium peaks shown in figure 3(c), were found to be 2.0 ± 0.6 nm and 4.6 ± 0.7 nm, respectively. Similar data for the QWs grown at the lowest temperature of 684 °C are shown in figure S2 of the SM. In that case peak indium content monotonically decreased from 25% for the QW furthermost from the sample surface to 22% for the topmost QW, and the average QW and QB widths were found to be 2.5 ± 0.3 nm and 6.6 ± 0.1 nm, respectively.

### 3.2. Emission properties

The normalised room-temperature PL spectra of the zb-InGaN/GaN QW samples are shown in figure 4(a); an absolute intensity comparison of the samples is given in figure S3 of the SM. The red shift of the QW emission as the QW growth temperature is reduced indicates a successful alteration of the indium composition within the QW layer. The FWHM of the QW emission, shown in figure S4 of the SM, varies between 0.29 eV and 0.34 eV as the growth temperature is altered. An oscillation of the peak intensity is clearly seen for photon energies less then ∼2.6 eV with a period of ∼0.06 eV. This period agrees well with the value calculated, using a previously described analysis [14], for Fabry–Perot fringe spacing of light reflecting between the air/GaN and the SiC/Si interfaces and using refractive indices for GaN and SiC of 2.45 [15] and 2.65 [16], respectively. The SiC begins to absorb significantly

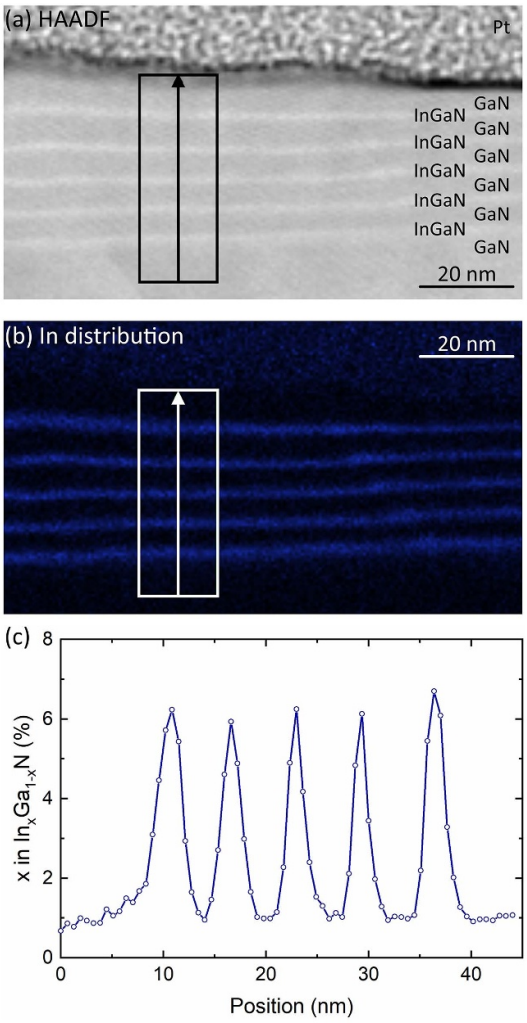


**Figure 3.** (a) HAADF image of QW sample grown at 740 °C. (b) EDX analysis of the same region shown in (a), with (c) a line scan taken across white arrow shown in (b).

for photon energies greater than ∼2.6 eV [17], suppressing the reflection from the SiC/Si interface and thereby the fringes. Figure 4(b) plots the chromaticity co-ordinates corresponding to the PL spectra shown in figure 4(a) and shows that varying the zb-QW growth temperature from 740 °C to 684 °C enables the perceived colour of the QW emission to be extended from the blue to the orange region of the visible spectrum.

Low-temperature power-dependent PL measurements were conducted on the samples to investigate the dependence of their PL spectra on excitation density, and the resulting normalised PL spectra are shown in figure 5. Irrespective of QW growth temperature, the peak QW emission spectra remain largely constant over the incident power density range investigated. As the incident power density increases, a slight reduction in relative intensity in the low energy tail of the QW emission can be observed clearly in figure 5(a) at 2.5 eV and (b) at 2.2 eV. Additional PL features around the 2.8–3.2 eV region are also visible in figure 5(d) (indicated by arrows) and are also weakly present in the QW samples grown at 706 °C and 693 °C in figures 5(b) and (c), respectively. The 2.8–3.2 eV features likely originate from the GaN barriers and resemble emission peaks observed in undoped zb-GaN epilayers [18]. The reduction in relative intensity of the 2.85 eV and 3.03 eV peak with increasing power density, observed in figure 5(d), indicate saturation of the emission processes in the GaN barrier. The PL spectra observed here for zb-QWs that are largely independent of the excitation density contrasts with the behaviour of wz-QWs. In the case of wz-QWs, a significant blueshift of the PL with increasing excitation density is commonly reported and attributed to screening of the internal polarisation fields [19–23]. For example, for a sample consisting of six 4 nm thick QWs with 15% indium content, a blue shift was reported for above gap excitation densities greater than 20 W $cm^{-2}$, with the peak energy increasing by 75 meV as

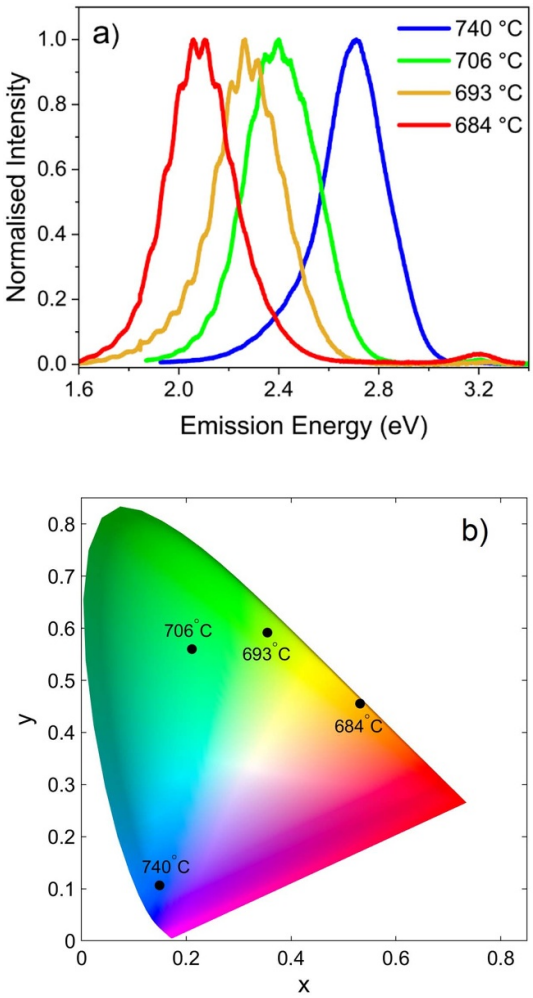


**Figure 4.** Room temperature PL spectra obtained from MOVPE grown zb-InGaN/GaN QWs as the QW growth temperature is altered (a), and the corresponding chromaticity coordinates in 1931 xy colour space (b).

the excitation was increased by factor of 100 beyond this threshold [23]. The lack of a significant blue-shift for these zb-QWs over a similar excitation range is consistent with the absence of polarisation fields expected for zb-QWs grown along the [001] direction [7].

Low temperature time decays of the peak QW emission energy are shown in figure S5 of the SM for all samples. Also shown in figure S5 are the associated 1/*e* lifetimes, which increase from 150 ps to about 400 ps as the growth temperature increases from 684 °C to 740 °C. The decrease in lifetime with lower peak QW emission energies (i.e. lower growth temperatures) is attributed to greater wave-function overlap between the carriers due to better confinement by the deeper QWs. Previous works have demonstrated sub-nanosecond 1/*e* lifetimes for blue [9, 24] and green-emitting zb-InGaN/GaN QWs [9] at low temperature. Figure S5 verifies these observations and demonstrates that fast recombination lifetimes are present in orange emitters. The sub-ns recombination lifetime in zb-InGaN/GaN QWs is attributed to the lack of QCSE and is in contrast to wz-QWs which exhibit recombination lifetimes that can be 100-fold longer and which increase significantly as the QW emission energy reduces [4, 25].

### 3.3. Effect of QW growth temperature on thermal quenching behaviour

Figure 6 shows the thermal quenching of the emission, relative to the intensity at low temperature, from the four zb-InGaN/GaN QW samples grown at different temperatures. The inset of figure 6 shows the 300 K relative intensities with bars representing the standard deviation of the intensity across the maps. Below 80 K all samples have broadly similar relative intensities with the relative intensity of each declining smoothly as the temperature rises. However, as the sample temperature is increased, the relative intensities of the samples quench at different rates and, whilst the decline in relative intensity remains smooth for the blue-emitting sample grown at 740 °C, the quenching of the others with increasing temperature is less smooth, particularly for the samples grown at 706 °C and 693 °C. By 300 K, the sample grown at 740 °C displayed the lowest relative intensity of 22%, intermediate QW growth temperatures

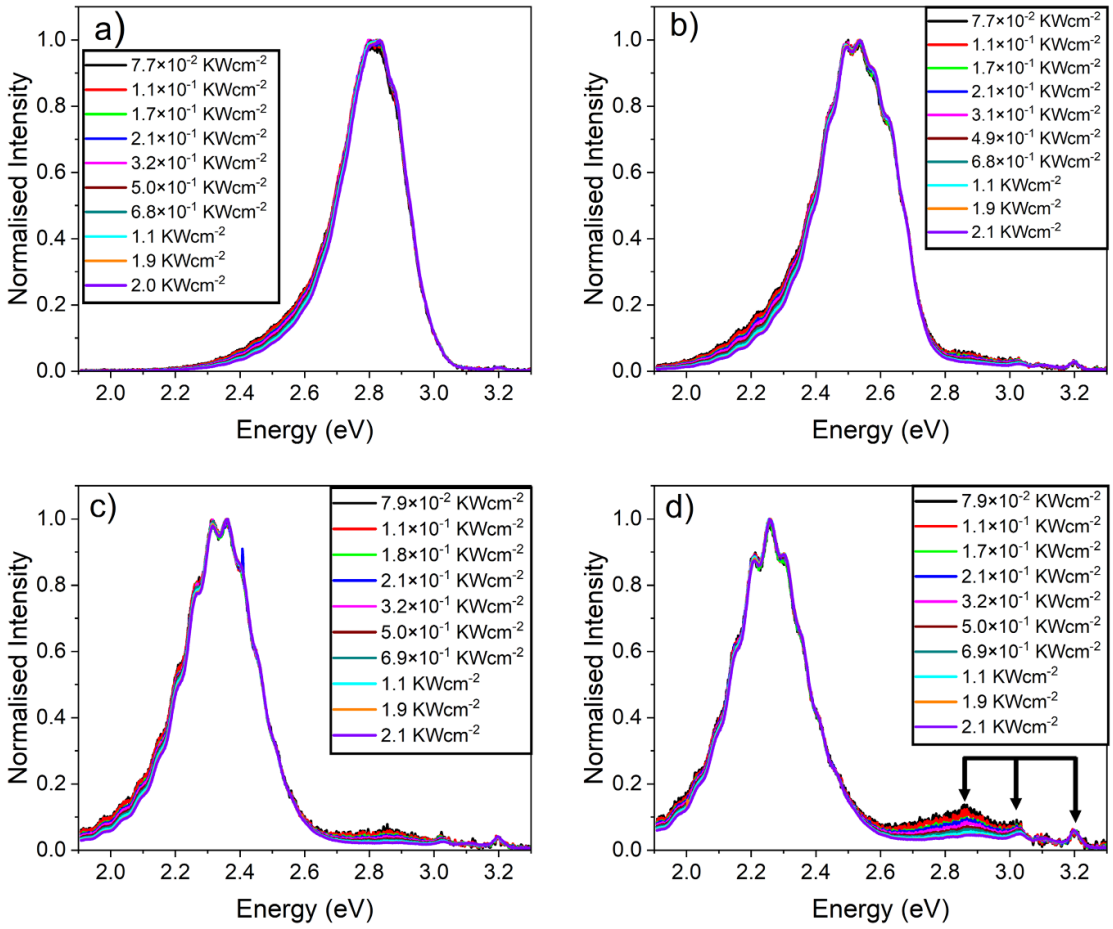


**Figure 5.** Normalised low temperature PL spectra as a function of incident power density for growth temperatures of (a) 740 °C, (b) 706 °C, (c) 693 °C and (d) 684 °C.

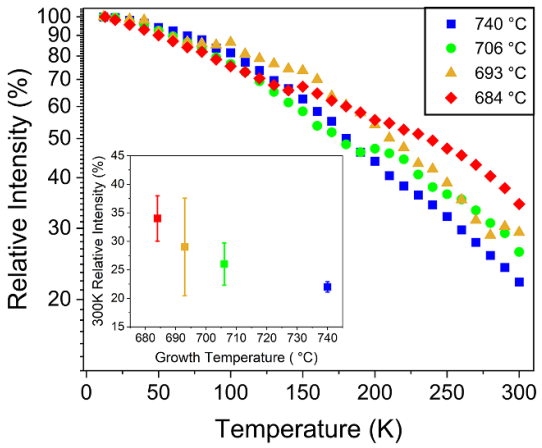


**Figure 6.** Thermal quenching of the zb-QW emission for different QW growth temperatures. Obtained using an incident excitation density of 10 W · cm$^{-2}$. Inset displays the 300 K relative intensities for the samples, with the error bars obtained from the standard deviation of the intensity across the PL maps.

of 706 °C and 693 °C had values of 26% and 29% respectively, and the QW sample grown at 684 °C exhibited the highest relative intensity of 34%. Thermally activated carrier escape from zb-QWs into the zb-GaN barriers has been reported to be a significant process that limits the room-temperature efficiency of blue-emitting zb-QWs [24]. This conclusion was based on the reduction in thermal quenching as the number and width of the QWs was increased, which both increase the probability that escaped carriers are recaptured by a QW. The observed improvement in relative intensity at 300 K for lower energy-emitting zb-QWs provides further evidence to support this theory; as the barrier height within the QWs

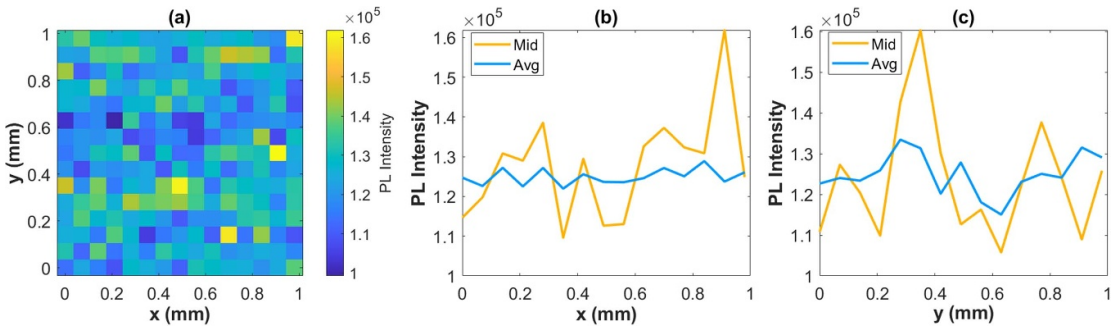


**Figure 7.** (a) Room temperature PL integrated intensity map of zb-InGaN/GaN QW sample grown at 693 °C, and the PL variation across the sample in the (b) x and (c) y dimensions. Note the map was taken across a 1 × 1 mm square surrounding the centre of the sample. This corresponds to the region targeted for excitation during spatially-integrated PL measurements.

increases for higher indium concentrations, carrier escape is reduced. However, as shown in figure S6 of the SM, thermal quenching measurements on the same samples can also produce results in which the relative intensity at 300 K is higher for the 706 °C sample than for the sample grown at 693 °C. The change in quenching behaviour between subsequent measurements is attributed to a variation in PL intensity across the samples. An example of the room-temperature PL variation for the QW sample grown at 693 °C is shown in figure 7, with the maps for the rest of the sample series shown in figures S7–S9 in the SM.

The intensity map, shown in figure 7(a), was produced by spectrally-integrating the QW emission obtained at each pixel on the map. The standard deviation of the pixel intensity was 10% of the average across the map. Line scans showing the intensity variation across the centre of the map (mid) and the average (avg) are shown for both the $x$ and $y$ dimensions of the map in figures 7(b) and (c) respectively, to identify trends and spot-to-spot variations across the sample. Note that the line scan for the centre of the samples is shown as this is the region of the sample excited during the PL measurements shown in figures 4–6. It can be observed that in the $x$-direction, there are intensity fluctuations from 1.15–1.60 × $10^5$ counts across the centre of the map, however, when the line scans are averaged across the $x$-direction, there is no clear trend. Looking at the variation in $y$, there are similar fluctuations in the midline values and an undulation in values in the average. The excitation spot used in figure 6 is comparable to the pixel size of figure 7. Therefore, between subsequent measurements on the 693 °C sample different spots near the centre of the sample could be getting excited each time, leading to significant changes in the QW integrated intensity at 300 K. Note spot-to-spot intensity variations of this scale are not present in the maps for the rest of the sample series.

## 4. Discussion

It has been shown that the emission energy of MOVPE-grown zb-InGaN/GaN QW structures can be tuned from the blue into the orange region of the visible spectrum by reducing the QW growth temperature from 740 °C–684 °C, indicating successful alteration of the indium content within the QW layer. This result is similar to a previous demonstration for MBE grown samples [11]. In that case the indium composition was varied from 3% to 30%, and the emission energy thereby tuned from 3.1 eV to 2.2 eV, by altering the growth temperature from 600 °C to 660 °C (or 500 °C to 560 °C for migration enhanced epitaxy). However, the next generation of LED displays requires pixels that can emit in the blue, green and red spectral regions, which indicates that to achieve red emission from MOVPE-grown zb-InGaN/GaN QWs the growth temperature of the QW layer must be reduced below 684 °C. There is nothing in the results presented to suggest that this will not be possible.

The QCSE present within wz-InGaN/GaN QWs reduces the electron-hole overlap function and also red shifts the emission. However, as the excitation density is increased, the carrier density within the wz-QWs increases, screening the electric field and leading to a blue shift of the QW emission. In contrast, figure 5 demonstrates that the zb-QW emission and FWHM remain largely constant as the incident excitation density is varied by over an order of magnitude and is attributed to the absence of polarisation fields in (001) zb-InGaN/GaN QWs, consistent with the work of Stark *et al* [6]. The excitation-density independence of the zb-InGaN/GaN QW spectra is a benefit to display applications because it ensures colour stability as the device brightness is altered.

Reduction in thermal quenching is observed as the QW emission energy is reduced. This trend can be explained by the thermionic escape of carriers from the QW layer having a significant effect on room-temperature efficiency. Thermionic escape is influenced by the band offsets between the GaN barrier and the InGaN QW layers. A recent theoretical study [26] calculated the conduction band (CB) and valance band (VB) offsets for unstrained zb-GaN and zb-InGaN as a function of indium content, with the methodology first validated against established results for wz-GaN and wz-InGaN. For 25% In, i.e. corresponding to the sample grown at 684 °C in this study, these calculations yielded CB and VB offsets for the zb phase of 0.63 eV and 0.30 eV, respectively, whilst for the wz-phase the values were each somewhat larger at 0.71 eV and 0.42 eV. It was also found [26] that the calculated band offsets scale broadly linearly with In content and so from this the CB and VB offsets for 5% In, i.e. corresponding to the sample grown at 740 °C, can be estimated, respectively, as 0.13 eV and 0.06 eV for zb phase and 0.14 eV and 0.08 eV for wz-phase. Quantum confinement can increase the energy of carriers in zb-GaN QWs considerably and thus lead to a greater rate of thermionic emission; a previous study on similar QWs reported an increase in the peak emission energy of 0.08 eV as the QW width was reduced from 7.5 nm to 2.5 nm [24]. The narrow QW widths used in this study will hence reduce the energy barrier for thermionic escape, with this reduction becoming increasingly significant as the growth temperature is increased and the band offsets decrease. However, the modest improvement in relative intensity at 300 K as the QW growth temperature reduces indicates that thermionic escape, whilst significant, is not the dominant process limiting the efficiency of zb-InGaN/GaN QWs at room temperature.

Significant variations in room temperature intensity are present across the QW sample grown at 693 °C, which impacts the value obtained in subsequent measurements on the sample. Note that spot-spot intensity variations of this magnitude are not present in the other samples in the series, see SM figures S7-S9. Zb-InGaN/GaN QWs are known to be rich in microstructural features such as stacking faults and wz inclusions [27–29] that can influence the emission properties [12, 13]. Variations in these microstructural features across the samples could lead to the observed spatial variability in room-temperature QW intensity. Scanning electron microscopy-cathodoluminescence measurements have proven to be an invaluable tool for investigating and assessing microstructural features in zb-QWs [29]. Employing this technique to the sample series studied in this article would elucidate the impact of QW growth temperature on microstructural features—an important consideration for low energy-emitting zb-LEDs.

## 5. Summary and conclusion

The effect of QW growth temperature on the emission properties of MOVPE-grown zb-InGaN/GaN QWs was investigated using PL techniques. Lowering the growth temperature of the QW layer from 740 °C to 684 °C tuned the room-temperature QW emission from blue to the orange region of the visible spectrum. The stability of the QW emission with increasing incident power density and the sub-nanosecond 1/*e* recombination lifetimes, regardless of QW growth temperature, verifies the absence of polarisation fields in the MOVPE-grown zb-InGaN/GaN QW samples. An overall reduction in thermal quenching is observed as the QW growth temperature is reduced, consistent with a reduction in thermionic escape of carriers from the QW layers into the zb-GaN barriers. However, the limited improvement in the room-temperature relative intensity with decreasing QW growth temperature indicates that thermionic escape is not the dominant process limiting the efficiency of zb-InGaN/GaN QWs at room temperature for these samples. The tunability of emission from the blue to orange and the stability of the emission spectrum over a range of excitation densities reported here indicate that LEDs based on zb-QWs have potential in display applications, which require both light output across the visible spectrum and colour stability as the display brightness is modulated. The sub-nanosecond recombination times observed here, which contrast with the 10–100 ns lifetimes typical of wz-QWs [30], means that zb-QWs are also well-suited to high data rate LiFi communications.

## Acknowledgments

The authors would like to acknowledge funding and support from the Engineering and Physics Sciences Research Council (EPSRC) under Grant Codes EP/W034956/1, EP/W035871/1 and EP/W03557X/1.

## Data availability statement

The data that support the findings of this study are openly available at the following URL/DOI: https://doi.org/10.48420/28770545 [31].

Supplementary Material available at https://doi.org/10.1088/1361-6463/ae4ef9/data1.

## ORCID iDs

D Dyer 0000-0003-2097-3689
M Frentrup 0000-0002-1726-3099
P Vacek 0000-0002-1625-9258
R A Oliver 0000-0003-0029-3993
D J Binks 0000-0002-9102-0941

## References

[1] Auf Der Maur M, Pecchia A, Penazzi G, Rodrigues W and Di Carlo A 2016 Efficiency drop in green InGaN/GaN light emitting diodes: the role of random alloy fluctuations *Phys. Rev. Lett.* **116** 027401
[2] Ren C X 2016 Polarisation fields in III-nitrides: effects and control *Mater. Sci. Technol.* **32** 418–33
[3] Tan A K, Hamzah N A, Ahmad M A, Ng S S and Hassan Z 2022 Recent advances and challenges in the MOCVD growth of indium gallium nitride: a brief review *Mater. Sci. Semicond. Process.* **143** 106545
[4] Hammersley S, Kappers M J, Massabuau F C P, Sahonta S-L, Dawson P, Oliver R A and Humphreys C J 2016 Effect of QW growth temperature on the optical properties of blue and green InGaN/GaN QW structures *Phys. Status Solidi c* **13** 209–13
[5] Chichibu S F *et al* 2003 Recombination dynamics of localized excitons in cubic $In_xGa_{1-x}N$/GaN multiple quantum wells grown by radio frequency molecular beam epitaxy on 3C–SiC substrate *J. Vac. Sci. Technol. B* **21** 1856–62
[6] Stark C J M, Detchprohm T, Lee S C, Jiang Y-B, Brueck S R J and Wetzel C 2013 Green cubic GaInN/GaN light-emitting diode on microstructured silicon (100) *Appl. Phys. Lett.* **103** 232107
[7] Elsaesser D R, Durniak M T, Bross A S and Wetzel C 2017 Optimizing GaInN/GaN light-emitting diode structures under piezoelectric polarization *J. Appl. Phys.* **122** 115703
[8] Vurgaftman I and Meyer J R 2003 Band parameters for nitrogen-containing semiconductors *J. Appl. Phys.* **94** 3675–96
[9] Chichibu S F, Onuma T, Sota T, DenBaars S P, Nakamura S, Kitamura T, Ishida Y and Okumura H 2003 Influence of InN mole fraction on the recombination processes of localized excitons in strained cubic $In_xGa_{1-x}N$/GaN multiple quantum wells *J. Appl. Phys.* **93** 2051–4
[10] Orozco Hinostroza I E, Avalos-Borja M, Compeán García V D, Zamora C C, Rodríguez A G, López L E and Vidal M A 2016 Tuning emission in violet, blue, green and red in cubic GaN/InGaN/GaN quantum wells *J. Cryst. Growth.* **435** 110–3
[11] Camacho-Reynoso M, Hernández-Gutiérrez C A, Yee-Rendón C M, Rivera-Rodríguez C, Bahena-Uribe D, Gallardo-Hernández S, Kudriavtsev Y, López-López M and Casallas-Moreno Y L 2022 Cubic $In_xGa_{1-x}N$/GaN quantum wells grown by migration enhanced epitaxy (MEE) and conventional molecular beam epitaxy (MBE) *J. Alloys Compd.* **921** 165994
[12] Church S A, Ding B, Mitchell P W, Kappers M J, Frentrup M, Kusch G, Fairclough S M, Wallis D J, Oliver R A and Binks D J 2020 Stacking fault-associated polarized surface-emitted photoluminescence from zincblende InGaN/GaN quantum wells *Appl. Phys. Lett.* **117** 032103
[13] Dyer D, Church S A, Ahumada-Lazo R, Kappers M J, Halsall M P, Parkinson P, Wallis D J, Oliver R A and Binks D J 2024 Efficiency droop in zincblende InGaN/GaN quantum wells *Nanoscale* **16** 13953–61
[14] Hums C, Finger T, Hempel T, Christen J, Dadgar A, Hoffmann A and Krost A 2007 Fabry-Perot effects in InGaN/GaN heterostructures on Si-substrate *J. Appl. Phys.* **101** 033113
[15] Köhler U, As D J, Schöttker B, Frey T, Lischka K, Scheiner J, Shokhovets S and Goldhahn R 1999 Optical constants of cubic GaN in the energy range of 1.5–3.7 eV *J. Appl. Phys.* **85** 404–7
[16] Shaffer P T B 1971 Refractive index, dispersion, and birefringence of silicon carbide polytypes *Appl. Opt.* **10** 1034
[17] Solangi A and Chaudhry M I 1992 Absorption coefficient of β–SiC grown by chemical vapor deposition *J. Mater. Res.* **7** 539–41
[18] Dyer D, Church S A, Jain M, Kappers M J, Frentrup M, Wallis D J, Oliver R A and Binks D J 2021 The effect of thermal annealing on the optical properties of Mg-doped zincblende GaN epilayers *J. Appl. Phys.* **130** 085705
[19] Takeuchi T, Sota S, Katsuragawa M, Komori M, Takeuchi H, Hiroshi Amano H A and Isamu Akasaki I A 1997 Quantum-confined Stark effect due to piezoelectric fields in GaInN strained quantum wells *Jpn. J. Appl. Phys.* **36** L382
[20] Kuroda T and Tackeuchi A 2002 Influence of free carrier screening on the luminescence energy shift and carrier lifetime of InGaN quantum wells *J. Appl. Phys.* **92** 3071–4
[21] Kuroda T, Tackeuchi A and Sota T 2000 Luminescence energy shift and carrier lifetime change dependence on carrier density in $In_{0.12}Ga_{0.88}N/In_{0.03}Ga_{0.97}N$ quantum wells *Appl. Phys. Lett.* **76** 3753–5
[22] Kazlauskas K *et al* 2005 Excitation power dynamics of photoluminescence in InGaN/GaN quantum wells with enhanced carrier localization *J. Appl. Phys.* **97** 0–7
[23] Kuokstis E, Yang J W, Simin G, Khan M A, Gaska R and Shur M S 2002 Two mechanisms of blueshift of edge emission in InGaN-based epilayers and multiple quantum wells *Appl. Phys. Lett.* **80** 977–9
[24] Church S A, Quinn M, Cooley-Greene K, Ding B, Gundimeda A, Kappers M J, Frentrup M, Wallis D J, Oliver R A and Binks D J 2021 Photoluminescence efficiency of zincblende InGaN/GaN quantum wells *J. Appl. Phys.* **129** 175702
[25] Li X, Pant N, DeJong E, Elshafiey A T, Armitage R, Kioupakis E and Feezell D 2023 Carrier dynamics in blue, cyan, and green InGaN/GaN LEDs measured by small-signal electroluminescence *Appl. Phys. Lett.* **122** 212108
[26] Tsai Y-C and Bayram C 2020 Band alignments of ternary wurtzite and zincblende III-nitrides investigated by hybrid density functional theory *ACS Omega* **5** 3917–23
[27] Ding B, Frentrup M, Fairclough S M, Kappers M J, Jain M, Kovács A, Wallis D J and Oliver R A 2020 Alloy segregation at stacking faults in zincblende GaN heterostructures *J. Appl. Phys.* **128** 145703

[28] Ding B, Frentrup M, Fairclough S M, Kusch G, Kappers M J, Wallis D J and Oliver R A 2021 Multimicroscopy of cross-section zincblende GaN LED heterostructure *J. Appl. Phys.* **130** 115705
[29] Gundimeda A *et al* 2025 Impact of stacking faults on the luminescence of a zincblende InGaN/GaN single quantum well *J. Appl. Phys.* **58** 025112
[30] David A and Grundmann M J 2010 Influence of polarization fields on carrier lifetime and recombination rates in InGaN-based light-emitting diodes *Appl. Phys. Lett.* **97** 1–4
[31] Dyer D *et al* 2026 Dataset for Wide tunability of zincblende InGaN/GaN quantum wells grown by metal-organic vapor phase epitaxy The University of Manchester Repository (https://doi.org/10.48420/28770545)